VDMA
Fluid Power Association

23rd ISC

International Sealing Conference

Stuttgart, Germany
Sept.30 - Oct.1, 2026

Sealing the future –
Facing the challenges of tomorrow

UNI STUTTGART

Fachverband Fluidtechnik im VDMA e. V. Lyoner Str. 18
50628 Frankfurt am Main
Germany

Phone +49 69 6603-1513
E-Mail maximilian.baxmann@vdma.eu

Internet www.vdma.eu/fluid

Impact of shaft lead on the tribological behavior of elastomeric rotary shaft seals

Mousa Amro, Bengt Wennehorst, Gerhard Poll, Max Marian

Depending on the manufacturing process, both micro and macro lead structures as well as combinations of both can be present on seal counterfaces. Due to viscous drag flow, these surface structures can cause additional axial fluid transport across the sealing contact, the direction of which depends on the structure angle and the rotation direction of the shaft. This superimposed secondary fluid transport caused by the counterface ("shaft pump rate") may substantially impair the reliable operation of elastomeric rotary shaft seals, which strongly depends on the reverse pumping effect due to viscous drag flow within the seal lip contact topography. When directed towards the air-side and exceeding the seal's reverse pump rate, a given shaft pump rate will likely cause leakage. In contrast, when directed to the oil-side, the additional reverse pumping of the shaft may reduce lubricant supply within the seal contact zone. Hence, due to the corresponding decrease in lubricant film thickness or even starvation, seal friction and contact temperature may rise substantially, and increased wear is to be expected. In the worst case, thermal damage of the seal lip may also cause leakage after only a short period of operation.

Within the scope of this contribution, 72 shafts provided by industry partners and characterized with micro and macro lead parameters (IMA Stuttgart) are examined tribologically. The investigations are conducted with plain elastomer lip seals made of FKM and NBR (diameters from 25 to 105 mm) and include the measurement of seal friction, seal and shaft pump rates, and leakage, as well as an evaluation of the wear behavior. Moreover, results from correlation analyses with the IMA lead and surface parameters are presented which provide additional information on which lead characteristics could be particularly harmful in terms of leakage.

1 Introduction

1.1 Fundamentals and state of the art

The seal counterface substantially influences the tribological conditions within the sealing contact. The standard manufacturing process for elastomeric rotary shaft seal counterfaces is plunge grinding with a rotating grinding wheel. Due to the complex processes occurring within the dynamic sealing gap and the resulting requirements for a suitable counterface, there are a variety of specifications, such as surface roughness, hardness, shaft geometry, and eccentricity [1], [2], [3], [4]. 2D and, increasingly, 3D parameters are used to specify surface topography. In most cases, roughness specifications are based on many years of empirical research or practical experience regarding the properties of suitable seal counterfaces. Under dynamic operating conditions and in the case of smooth moulded seal lips, counterfaces that are too smooth may prevent the initial run-in of the seal lip. This, however, represents a precondition for the formation of the necessary lubricating film within the sealing contact zone. Surfaces that are too rough can have an abrasive effect and increase seal lip wear. A seal counterface that is "too smooth" or "too rough" is, therefore, detrimental to the sealing system. In sealing technology, the term “harmful structures” refers to all types of surface structures that have a detrimental effect on the sealing function. Various forms of harmful structures may be found on seal counterfaces. In addition to surface roughness that is unsuitable for use as a seal counterface, these can include, for example, scratches, dents, or rust. The effects of stochastic seal counterface structures, such as scratches or dents, were investigated by Leis and von Hollen [5] as well as Matus and Poll [6], 0, [8].

While defects such as scratches or dents are caused mostly due to inattention when handling the component after the manufacturing process or during transport, lead structures on the seal counterface are created during surface production. The issue of “lead on shaft seal counterfaces” is not a new one. As early as the 1950s, initial publications [9] pointed to an axial fluid transport effect caused by the seal counterface, which leads to the failure of sealing systems. Since then, various methods for measuring lead have been investigated. One of the oldest and simplest methods is the thread method [4]. Thereby, the component to be measured is clamped horizontally. A weighted thread is positioned around the seal counterface, which is then set in rotation. If an axial force acts on the thread, it moves in the axial direction. If this behavior occurs in the opposite direction after a reversal of the direction of rotation, a lead structure is present on the seal counterface. For a long time, this simple approach was the only way to assess lead, at least in qualitative terms. The first quantitative analysis of macro-lead was conducted in 1997 using the Computer Aided Roughness Measurement and Evaluation (CARMEN) method [10], [11], [12]. The latter detects periodic macro-lead, but can’t detect micro-lead due to the method's low resolution in the circumferential direction of the shaft.

However, Raab [13], Kunstfeld [14], Buhl [15], and Jung [16] demonstrated that extremely small and finely oriented microstructures (micro-lead) generate a substantial axial fluid transport effect. Against this background, *Baitinger* and *Baumann* [17], [18], [19] developed a method for detecting and analyzing micro-lead, which has since been brought to market. Optical topography instruments are used to gain the required high resolution to capture microstructures. Using digital image processing and statistical methods, the captured microstructures are segmented and analyzed in terms of their number, orientation, structural depth, volume, and geometric position. Subsequently, *Engelfried*, *Baumann*, and *Bauer* developed a structure-based method for the 3D analysis of macro-lead [20].

The different types of lead can be categorized, for example, based on their magnitude, [21], [22]. These harmful structures may be directional or non-directional and may be present in specific areas or across the entire surface. One of the various types of lead is what is known as micro-lead. Micro-lead is characterized by randomly arranged, anisotropic structures that result from a multitude of grinding marks created during the manufacturing process. Micro-lead can be caused by misalignment between the grinding wheel and the shaft axis. The structural length is determined by the grain contact length during the grinding process and also depends on the diameter of the seal counterface. Because micro-lead structures are so narrow (often less than 20 µm), a relatively large number of microstructures in the narrow seal lip contact region contribute to fluid transport, which can result in a high overall axial fluid transport effect.

Another type of lead is what is known as macro-lead. Macro-lead consists of macroscopic structures that can form as a result of the dressing process of the grinding wheel during the manufacturing of the seal counterface. The macroscopic structures formed in this way are axially periodic and predominantly circumferential, similar to a screw thread. The size of these macroscopic, axially periodic structures typically ranges from 20 µm to 800 µm in width. This can be attributed to dressing marks on the grinding wheel caused by the dressing process using a single point diamond dressing tool. Transferring the dressing spiral formed during dressing with a single point diamond dressing tool to the grinding wheel results in a kind of helical pattern on the workpiece surface. The formation of macro-lead depends strongly on the dressing conditions and the speed ratio during the grinding process. It is advisable to avoid speed ratios that are whole or half numbers.

In practice, the various types of harmful structures are usually not found individually on the seal counterface, but appear superimposed on the surface, with varying degrees of intensity and in different directions. For example, a micro-left-hand lead and a macro-right-hand lead can coexist on the same surface. The individual effects superimpose and influence the complex processes taking place within the dynamic sealing gap.

The seal counterface is a critical component in the rotary shaft seal tribological system, comprising three primary elements: the seal, the counterface, and the fluid to be sealed. The individual elements of the sealing system must be carefully coordinated to ensure reliable operation, as they interact in complex ways during operation. The properties of the seal counterface affect the friction, wear, and sealing performance of the rotary shaft seal. Fundamentally, a distinction can be made between static and dynamic sealing, which are based on different mechanisms. Static tightness refers to the condition of the system when the shaft is at a standstill and dry contacts between the elastomer seal lip topography and the counterface prevent the lubricant from leaking through the sealing contact. Under dynamic conditions, relative motion occurs between the seal lip and the counterface. The processes occurring in the sealing gap during dynamic operation are highly complex. Due to the relative motion of the seal counterface, lubricant is dragged into the sealing contact topography, causing the elastomer surface to be supported and separated from the counterface—on different length scales—by a micro-elastohydrodynamic lubricating film [23], [24], [25], see Figure 1.

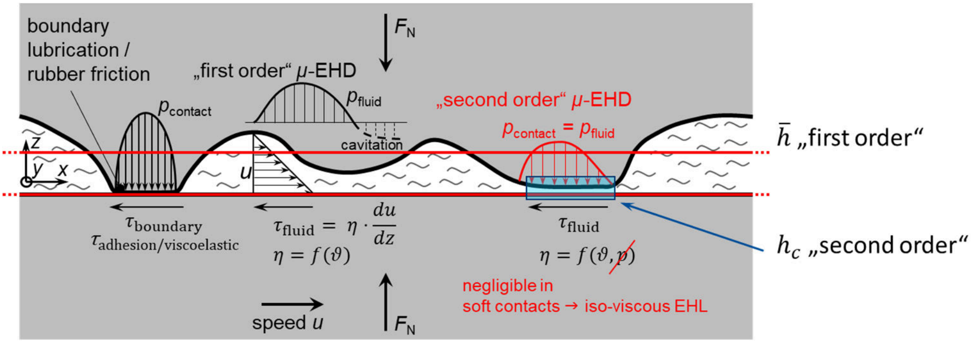

Figure 1: Elastomeric rotary shaft seal lubricant film formation mechanisms and friction regimes [23], [24], [25]

At the same time, the seal's active reverse pumping action prevents this lubricating oil from leaking. There are various complementary functional models that describe the reverse pumping effect of elastomeric rotary shaft seals, such as the distortion hypothesis, or the side-flow hypothesis, see, e. g., [26], [27].

Depending on the manufacturing process, both micro and macro-lead structures as well as combinations of both can be present on the seal counterface. Due to viscous drag flow, these surface structures can cause additional axial fluid transport across the sealing contact, the direction of which depends on the structure angle and the rotation direction of the shaft. This superimposed secondary fluid transport caused by the counterface ("shaft pump rate") may substantially impair the reliable operation of elastomeric rotary shaft seals, which strongly depends on the reverse pumping effect due to viscous drag flow within the seal lip contact topography. When directed towards the air-side and exceeding the seal's reverse pump rate, a given shaft pump rate will likely cause leakage. In contrast, when directed to the oil-side, the additional reverse pumping of the shaft may reduce lubricant supply within the seal contact zone. Hence, due to the corresponding decrease in lubricant film thickness or even starvation, seal friction and contact temperature may rise substantially, and increased wear is to be expected. In the worst case, thermal damage of the seal lip may also cause leakage after only a short period of operation.

1.2 Aims and scope

Using the aforementioned surface analysis methods, lead structures can be detected and characterized. However, for real-world industrial shafts, these parameters have not yet been evaluated extensively with regard to sealing system performance in terms of friction and leakage. Following up on previous research [28], the investigations included measurements of seal friction, shaft pump rates, and leakage, as well as an assessment of the wear behavior. While these investigations were initially intended to describe the functional behavior of the various seal counterfaces and sealing systems based on a large experimental dataset, the broader objective was to address the following overarching questions:

1. Is it possible to develop an experimental screening method to detect critical seal counterfaces based on differences in friction behavior during clockwise (cw) and counterclockwise (ccw) rotation?
2. How do the measured shaft pump rates correlate with the lead parameters and other surface characteristics determined in the surface analyses? Can threshold values be derived to distinguish between acceptable and unacceptable seal counterfaces?

2 Materials and methods

2.1 Sealing systems examined and general experimental conditions

Within the scope of this contribution, 72 shafts provided by industry partners and characterized with micro and macro lead parameters (IMA Stuttgart) were examined tribologically, see table 1. The investigations were conducted with plain elastomer lip seals (DIN 3760 Type A, i. e., no dust excluder lip) made of fluorocarbon rubber (FKM) and nitrile butadiene rubber (NBR), with sealing diameters ranging from 25 to 105 mm. The FVA reference oil FVA3 (mineral oil without any additives) was used as a lubricant.

Table 1: Counterface characteristics

Designation	Sealing diameter (mm)	Lead characteristic
CF25	25	Micro-lead
CF35	35	Macro-lead, Combined Micro-Macro-lead
CF50	50	Micro-lead, Combined Micro-Macro-lead
CF80	80	Macro-lead, Combined Micro-Macro-lead
CF90	90	Micro-lead
CF100	100	Macro-lead
CF105	105	Macro-lead

2.2 Seal friction measurement

To determine the friction torque of a sealing system, the seal pump rate test rig (custom-made) shown in Figure 2 was used. The tested counterface was connected to the test rig's spindle via an adapter. The friction torque of the sealing system and the spindle bearings was measured using a high precision torque measurement shaft (Dataflex 16/10, KTR; measuring range of 2 Nm) installed between the test spindle and the electric motor. After a test, the measured total friction torque was corrected for bearing friction using a correction table. The vented test head was filled with lubricant up to the center of the shaft. The lubricant temperature was measured using a thermocouple and controlled to 80 °C by heating elements located in the wall of the test head. A scale placed beneath the drain opening of the test head on the air-side of the sealing system recorded any leakage from the test seal with temporal resolution. With this setup, it was also possible to measure the pump rate of a radial lip seal by installing the seal in reverse (see also section 2.3). The data acquisition system recorded the measured variables (friction torque, oil sump temperature, rotational speed, drip weight) at a sampling rate of 1 kHz and calculated an average value from every 100 data points, which was then stored at a storage rate of 5 Hz.

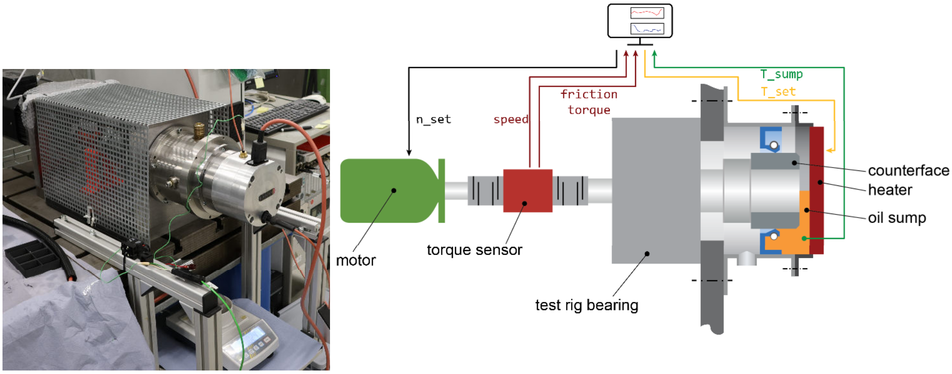

Figure 2: Test rig for measuring seal friction and seal pump rates.

Preliminary experiments showed that larger differences in the friction torque depending on the direction of rotation tended to be observed at lower sliding speeds. Since substantially thinner lubricant films are to be expected under these conditions, the influence of lead structures on the lubrication state was likely to be greater and, thus, more clearly visible in the friction torque measurement. In further experiments in which the length of the rotation direction intervals was varied, repeatable trends in the friction torque did not emerge until after several changes in rotation direction. Based on these findings, the experimental procedure shown in Figure 3 was developed. This consisted of a half-hour preconditioning phase, during which the test head was heated to the pre-set temperature while at rest. This was followed by a ten-hour run-in of the sealing system at the highest sliding speed to be tested, with several changes in the direction of rotation. The initial direction of rotation was chosen so that both, the seal counterface and the seal, would pump the oil inward (i. e., towards the oil-side), thereby tending to cause starved lubrication or dry running of the sealing contact. The pumping direction of the counterface was determined based on the orientation of the surface structures. For systems with micro- and macro-lead oriented in opposite directions, the results of the pump rate measurements were used. The sliding speeds to be tested were then run through in descending order, with each sliding speed being maintained for a total of 4 hours. During this time, the direction of rotation was changed several times at 30- or 60-minute intervals. This resulted in a total duration of 26.5 hours for an experiment.

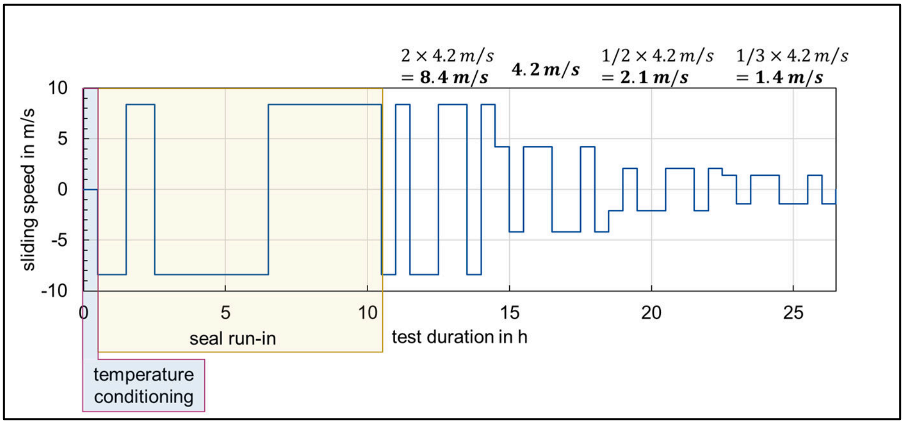

Figure 3: Test procedure for measuring seal friction.

The sealing systems were tested at a sliding speed of 4.2 m/s (based on previous observations [28]) as well as at speeds equal to twice (8.4 m/s), half (2.1 m/s), and one-third (1.4 m/s) of that speed. However, due to resonance vibrations, the rotational speed required to achieve a sliding speed of 8.4 m/s at smaller nominal diameters was not reached. For this reason, this higher sliding speed was not investigated for seal sizes 25 and 35 mm. In these cases, the run-in speed was 4.2 m/s. The further test conditions for the friction torque measurements are summarized in Table 2.

Table 2: Test conditions for the friction torque measurements

Seal material	FKM
Seal orientation	Oil-side facing oil sump (regular installation)
Initial direction of rotation	Counterface and seal pumping inward (towards oil-side), thereby tending to cause starved lubrication
Test duration	26.5 h (22.5 h for samples CF25 and CF35)

To evaluate a test, the average friction torque for the last 5 minutes of an operating point was calculated. For further analysis, however, the last of these average values from each speed step was used for both directions of rotation. Finally, the seal friction in the outward pumping (i. e., leakage) direction was subtracted from that in the inward pumping direction, and this difference in friction torque was used to compare the sealing systems.

2.3 Pump rate measurements and leakage investigations

To determine the shaft pump rates and investigate the leakage behavior, custom-made endurance seal test rigs as shown in Figures 4 and 5 were used. These allowed the simultaneous testing of four sealing systems on each of six test stations, with the test parameters oil sump temperature, rotational speed, and runtime being independently adjustable for each position. In this setup, the test seal was pressed into the lid of the test head, and the counterface to be investigated was mounted on a fixture directly driven by an electric motor. The test head was filled with lubricant up to the shaft center, and the oil sump was temperature-controlled to 80 °C via a resistance thermometer and a heating sleeve on the outer wall. The onset and further progression of leakage were monitored using cameras and performing subsequent image analyses. The amount of leakage was determined both volumetrically and gravimetrically. To measure the pump rate, the test seal was installed in reverse, so that its air-side was flooded with lubricant. The pumped lubricant was collected in a reservoir, whose mass was recorded over time using a laboratory balance (Kern) and stored. From this data, the pump rate for each operating point can be determined after a test based on the temporal change in the pumped lubricant quantity.

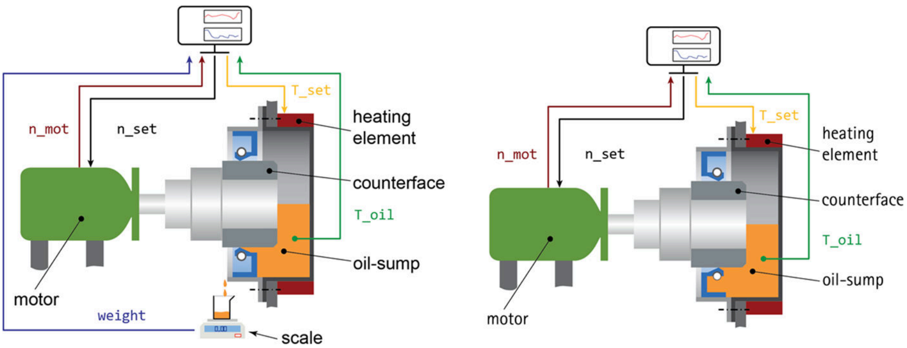

Figure 4: Schematic setup of the endurance seal test rigs for measuring the pump rate (left) and investigating leakage behavior (right).

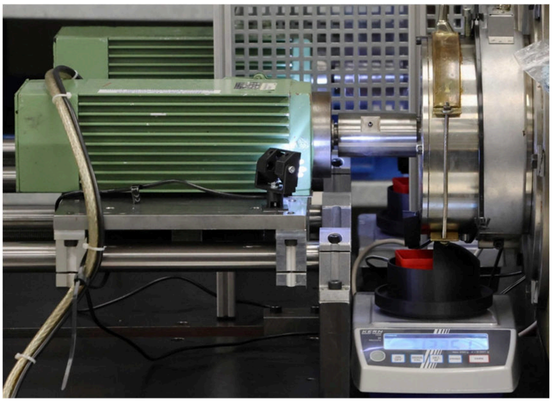

Figure 5: Photo of one of the endurance seal test rig positions.

2.3.1 Leakage investigations

To investigate the sealing systems for their functionality, leakage tests were conducted. The direction of rotation was selected based on the respective lead pattern such that the surface structures drag the lubricant outward against the reverse pumping effect of the seal. For counterfaces featuring both micro- and macro-lead patterns in opposing orientations, both shaft rotation directions were investigated. An overview of the test conditions is provided in Table 3.

Table 3: Test conditions for the leakage tests

Seal material	NBR, with supplementary single tests using FKM
Seal orientation	Oil-side facing oil sump (regular installation)
Direction of rotation	Selected to promote leakage (outward pumping)
Test cycle	24 h at 4.2 m/s, followed by an additional 24 h at 8.4 m/s if no leakage occurs

2.3.2 Pump rate measurements

To quantify the pumping behavior of the lead structures, pump rate measurements were conducted using FKM seals, with supplementary tests performed using NBR seals. For this purpose, the test seal was installed in reverse (air-side facing the oil sump), and the counterface was operated in both directions of rotation. The test procedure is shown in Figure 6.

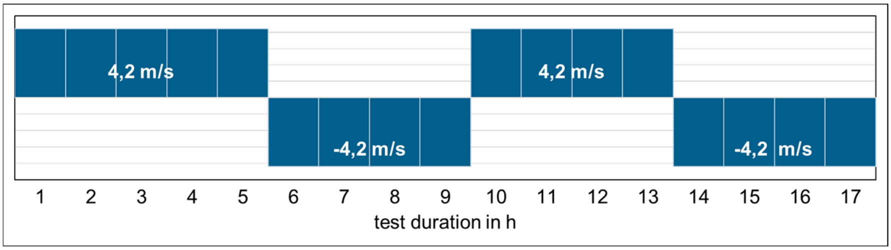

Figure 6: Test procedure for determining the pump rate

The pump rates were determined at a sliding speed of 4.2 m/s. After a one-hour run-in phase, each direction of rotation was maintained for 4 hours, with each direction being approached twice. An overview of the test conditions is provided in Table 4.

Table 4: Test conditions for the pump rate measurements

Seal material	FKM, with supplementary single tests using NBR
Seal orientation	Air-side facing oil sump (reverse installation)
Direction of rotation	Alternating (cw/ccw) to assess bidirectional pumping behavior
Test duration	17 h

The pump rate of the sealing system was determined after a test by calculating the slope of the time-resolved curve of the gravimetrically measured pumped quantity for each operating point. The shaft pump rate PR_{CF} was then calculated from the system pump rates $PR_{Sys,cw}$ and $PR_{Sys,ccw}$ of both directions of rotation [28]:

$$PR_{\mathrm{CF}} = \frac{1}{2}\left(PR_{\mathrm{Sys,cw}} - PR_{\mathrm{Sys,ccw}}\right). \quad (1)$$

3 Results and discussion

3.1 Friction measurements

Differences in the frictional behavior of the seals were observed between different counterface sizes and within a single size category. For example, while the temporal frictional behavior of the CF100-05 system (Figure 7) exhibited a smooth profile with stable steady-state values at each speed level, this was not the case for the CF100-06 system (Figure 8). For the latter, the profile exhibited pronounced instabilities and an elevated friction level at low sliding speeds. Similar behavior was particularly observed in the CF25 and CF80 systems. The direction-dependent differences in friction torque (see section 2.2) are summarized in Figures 9 and 10 for all sealing systems. The observed differences clearly indicate that lead structures affect seal friction, with friction typically being higher during reverse-pumping rotation. This can be explained by the fact that, in this direction of rotation, the lead structures partially drag lubricant out of the dynamic sealing gap, thereby reducing the lubricant film thickness. Furthermore, a frequently observed dependence of the frictional torque difference on sliding speed is illustrated in these figures. In the CF35-07 system (Figures 9 and 11), it is exemplarily shown that the friction torque difference increased with decreasing sliding speed, while the total friction torque decreases. Under these operating conditions with reduced micro-elastohydrodynamic lubricant film thickness, the surface topography of the counterfaces appeared to have an increasing influence on the overall seal friction, possibly due to enhanced interaction between the surface structures/asperities and the elastomeric seal material. This comparatively higher friction difference was particularly seen at elevated temperatures and the corresponding lower lubricant viscosities and film thicknesses. As shown in Figure 11, no differences between the two directions of rotation were observed during operation without temperature control, i.e., with the correspondingly higher lubricant viscosities. In systems that do not follow the aforementioned observations, increased instabilities in the friction curves and, in some cases, substantial leakage (e.g., system CF90) occurred.

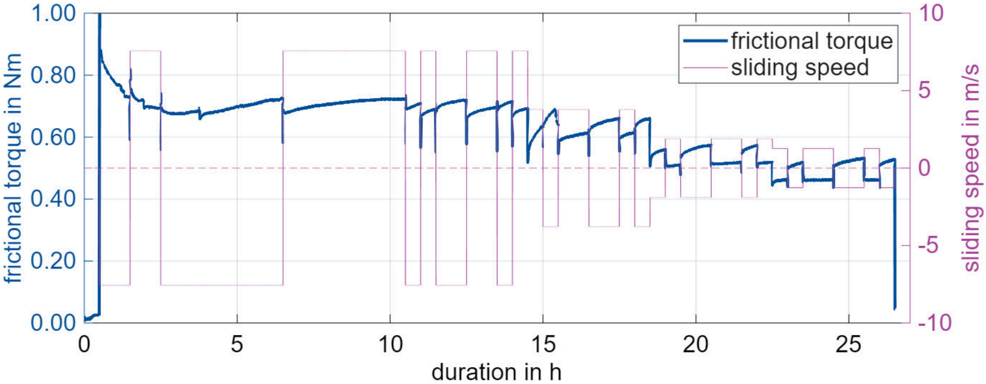

Figure 7: Frictional behavior of the CF100-05 system

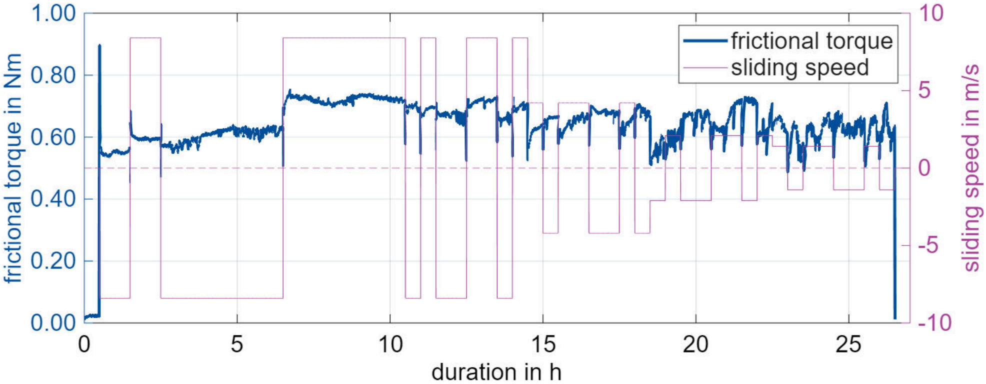

Figure 8: Frictional behavior of the CF100-06 system

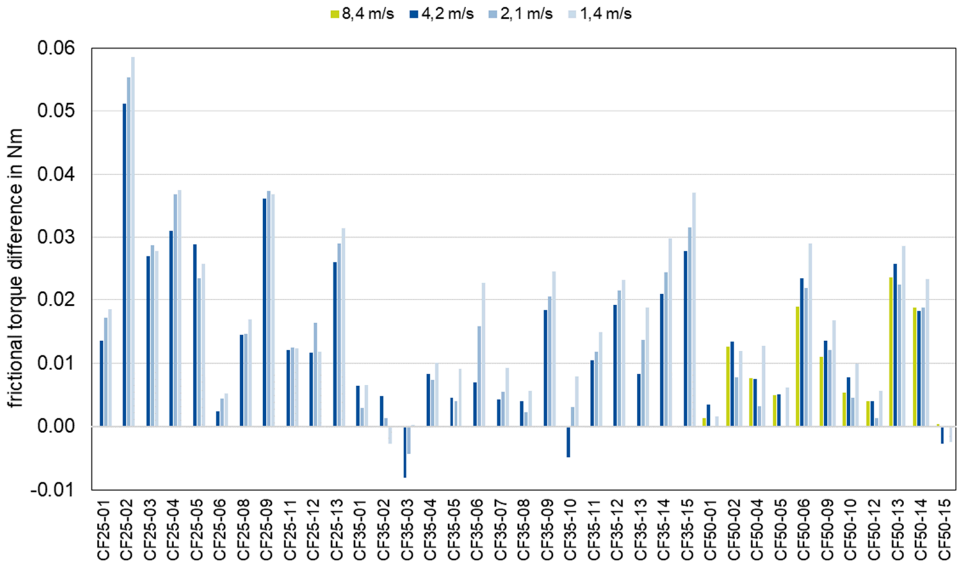

Figure 9: Difference in seal friction between the reverse-pumping and leakage-promoting directions of rotation; systems CF25, CF35, and CF50

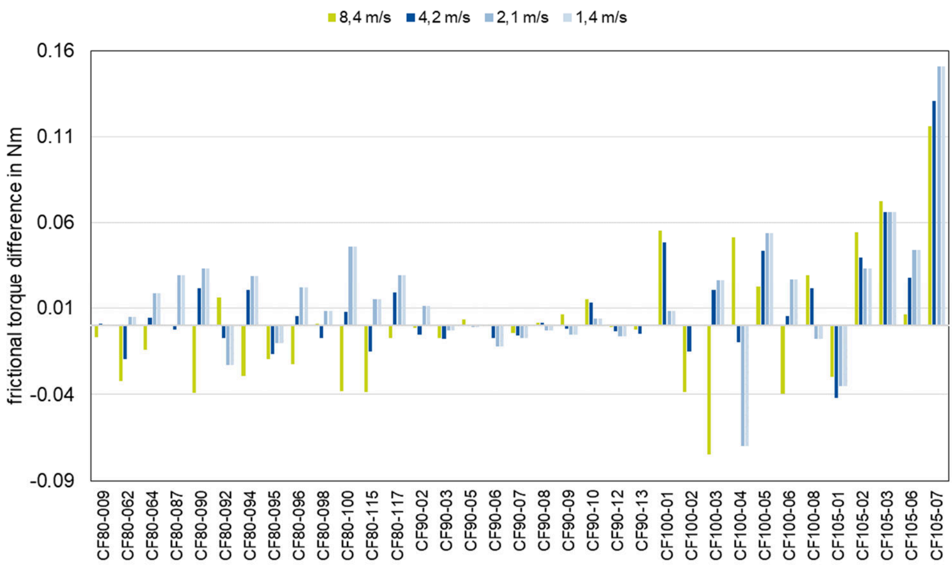

Figure 10: Difference in seal friction between the reverse-pumping and leakage-promoting directions of rotation; systems CF80, CF90, CF100, and CF105

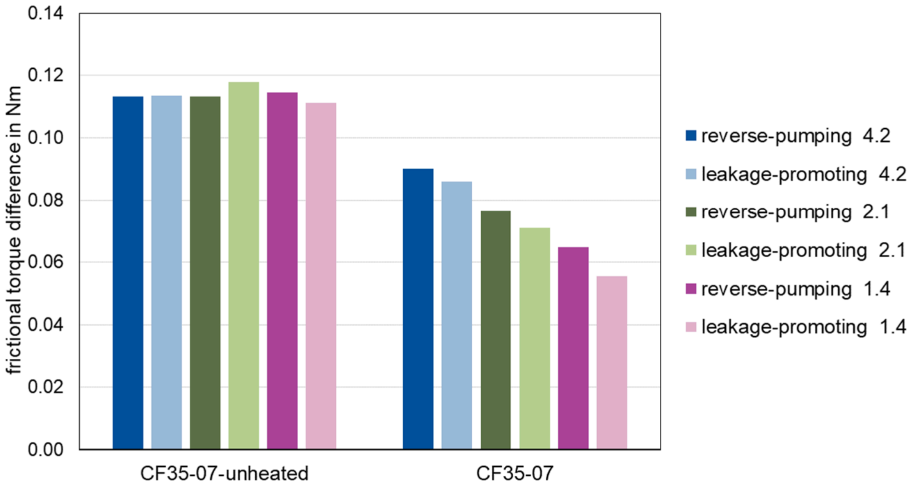

Figure 11: Seal friction in the reverse-pumping and leakage-promoting directions of rotation; system CF35-07 without temperature control (oil sump equilibrium temperatures between 30 and 50 °C) and with temperature control (oil sump temperature = 80 °C)

3.2 Leakage and wear assessment

The FC90 counterfaces exhibited particularly notable leakage behavior, with leakage beginning after a short runtime of approximately 4 hours. Depending on the counterface, leakage ranged from 12 to 70 g at the end of the test. Additional counterfaces where leakage occurred, also after a short runtime, included: All counterfaces of size CF100, as well as two counterfaces each of sizes CF25 and CF50. However, these systems remained only oil-wet or showed a comparatively low leakage quantity of at most 4 g (CF50: leakage only in left-hand rotation, right-hand rotation leakage-free). When the CF90 systems were additionally tested with FKM seals, they remained leakage-free in both directions of rotation. This was consistent with the leakage behavior observed in the friction measurements (also using FKM seals), where none of the different systems exhibited leakage. This can be attributed to the reverse pump rates of the FKM seals being considerably higher than those of NBR seals, as demonstrated in previous investigations [28].

The CF90 system exhibited the lowest seal lip wear. The latter was more pronounced in sealing systems with smaller diameters, which might be related to thermal scale effects (i.e., higher sealing contact excess temperatures) within the sealing contact zone. When the system CF25-02 was additionally tested in the reverse-pumping direction of rotation with the lead structures also dragging the lubricant towards the oil-side, increased wear was observed.

3.3 Pump rate measurements

Following the test procedure shown in Figure 6, each direction of rotation was approached twice. The pump rates decreased with increasing number of directional changes. This phenomenon was already previously reported [28] and attributed to the run-in behavior of the sealing systems. For further analyses, the shaft pump rate was calculated based on the last measured system pump rate in each direction of rotation. Supplementary single shaft pump rate measurements were conducted with NBR seals. However, due to the substantially weaker pumping capacity of the NBR seals, only a few drops were recorded during some of these tests over the course of an experiment, resulting in considerably higher uncertainties in the determination of the shaft pump rates.

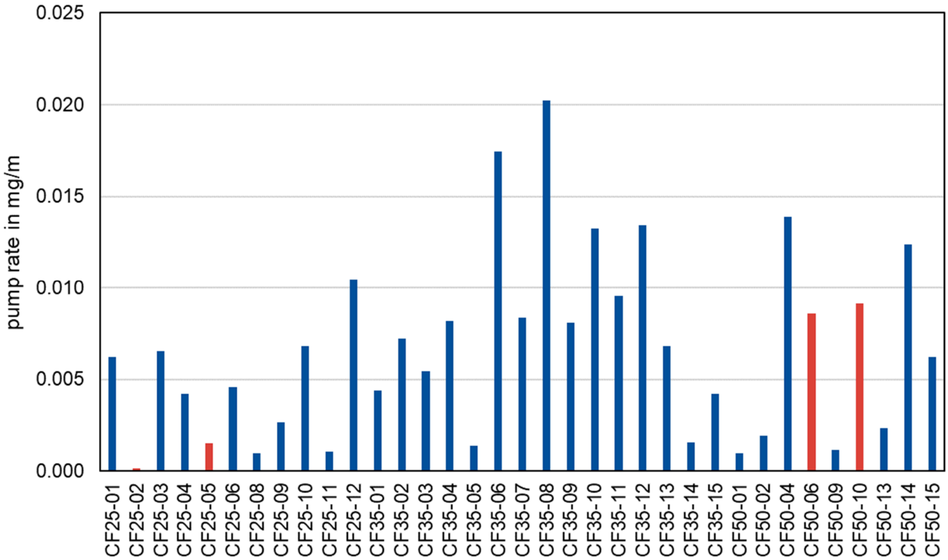

Figure 12: Shaft pump rates of the CF25, CF35, and CF50 systems (color coding indicating leakage test results: blue = leak-free systems, red = systems with leakage)

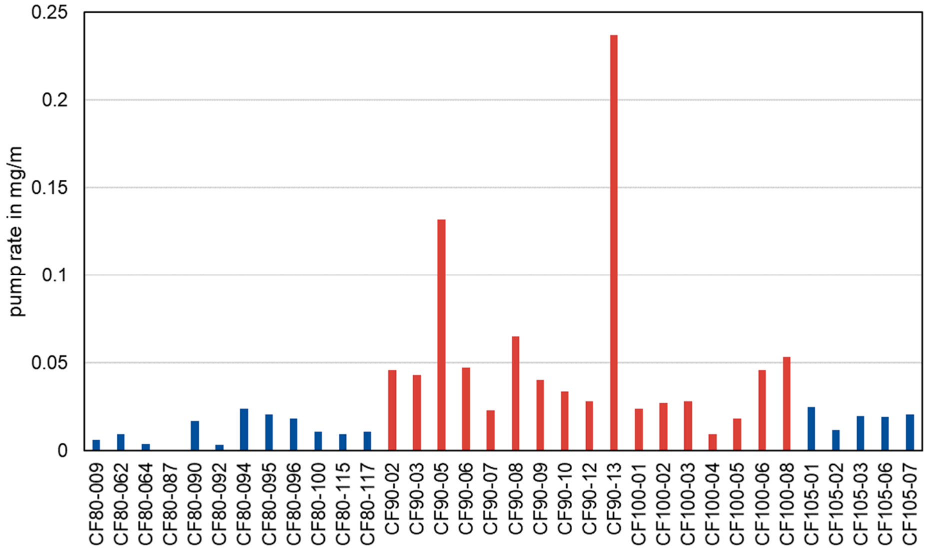

Figure 13: Shaft pump rates of the CF80, CF90, CF100, and CF105 systems (color coding indicating leakage test results: blue = leak-free systems, red = systems with leakage)

The shaft pump rates measured with FKM seals are illustrated in Figures 12 and 13. In these figures, the colors represent the results of the leakage investigations: Blue-marked systems remained leak-free, while red-marked systems exhibited leakage. This representation clearly demonstrates the particularly high pump rates of the counterfaces in the CF90 and CF100 systems, which may explain the leakage behavior of these systems. However, the leaking counterfaces of sizes CF25 and CF50 did not exhibit notably high pump rates.

3.4 Correlation analyses

Regarding the macro-lead counterfaces (systems CF35, CF50, CF80, CF100, and CF105), the MBN31007-7 [12] (see section 1.1) macro-lead parameters *DP* (lead period length), *Dt* (lead depth), and *Dy* (lead angle) aligned with previous analyses [20], [28], resulting in a linear correlation between shaft pump rates and the group $-Dy \cdot Dt/DP$. When using the structure-based 3D analysis method [20], comprising the macro-lead parameters SDB_{mean} (average structure width), SDT_{mean} (average structure depth), SDy_{mean} (average structure angle with 0° corresponding to the circumferential direction), and the corresponding group $-SDy_{mean} \cdot SDT_{mean}/SDB_{mean}$, the coefficient of determination increased from 0.684 to 0.804. This can be attributed to the fact that the structure-based evaluation considered individual features, which are filtered out in the periodic analysis of the MBN31007-7. Within the scope of this study, it was not possible to identify specific macro-lead parameters or thresholds thereof that could be indicative of unacceptable, i.e., leaking counterfaces. This might be related to the fact that leakage in these systems was comparatively low and limited to the air-side meniscus of the seal being oil-wet, without exhibiting severe dripping leakage comparable to that of the CF90 micro-lead system.

To further analyze the influence of micro-lead on the shaft pump rate and the leakage behavior, the shaft pump rates of the micro-lead counterfaces (systems CF25 and CF90) were first correlated with the individual micro-lead and surface parameters in numerous comparisons. This revealed the correlation shown in Figure 14 between the absolute value of the arithmetically averaged micro-lead angle Sd_{mean} and the leakage behavior. It was observed that micro-lead counterfaces exhibiting notable leakage had an Sd_{mean} of over 0.1 ° as well as shaft pump rates exceeding 0.02 mg/m. However, this range of Sd_{mean} also contained a few counterfaces with lower shaft pump rates that exhibited no or only minor dripping leakage (system CF25 being only oil-wet). Additionally, a notable pattern between the surface parameter Sz_{mean} (average areal maximum height) and the leakage behavior was identified during further analyses of the surface parameters, see Figure 15. It was observed that micro-lead counterfaces with an Sz_{mean} of approximately 2.5 µm or higher exhibited oil-wet sealing contacts or minor dripping leakage (system CF25). The severely leaking CF90 systems exhibited markedly larger Sz_{mean} values between 2.8 and 3.5 µm. The shaft pump rates of these systems were all above 0.02 mg/m. Whether these simple thresholds can already help predict leakage in micro-lead shafts requires further investigation.

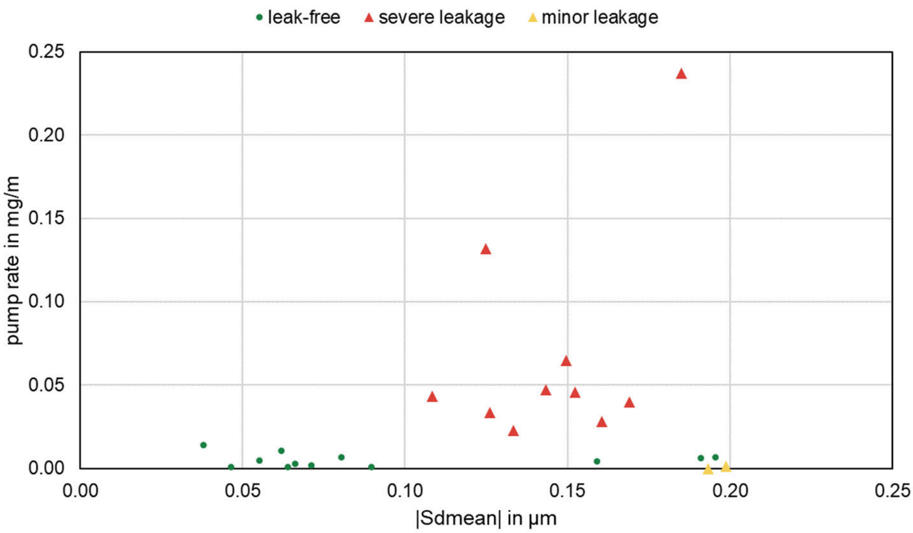

Figure 14: Absolute value of Sd_{mean} vs. shaft pump rates

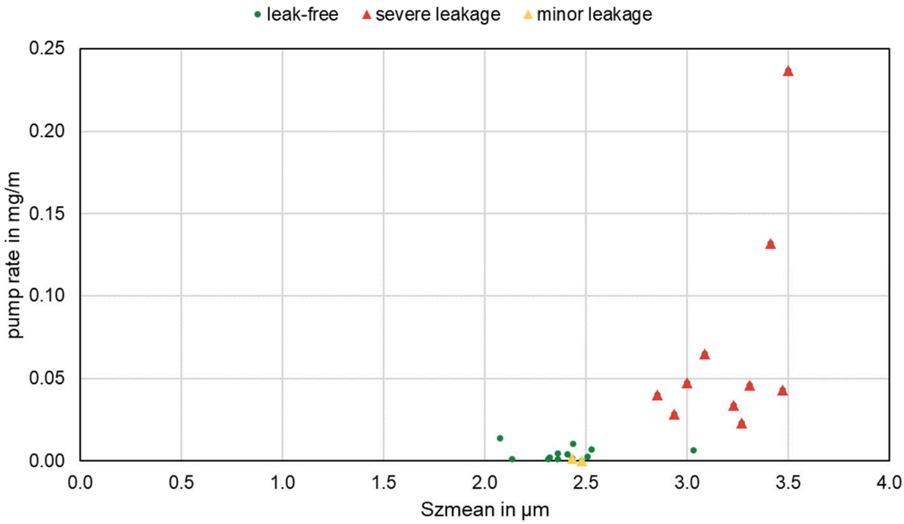

Figure 15: Average areal maximum height Sz_{mean} vs. shaft pump rates

4 Summary and conclusions

Within the scope of this contribution, 72 shafts with micro and macro lead parameters were examined tribologically. The investigations were conducted with plain elastomer lip seals made of FKM and NBR (diameters from 25 to 105 mm) and included the measurement of seal friction, shaft pump rates, and leakage, as well as an assessment of the wear behavior. Moreover, results from correlation analyses with lead and surface parameters were presented, providing additional insights into which lead characteristics may be particularly detrimental to sealing performance.

Coming back to the overarching questions formulated in section 1.2, the results showed that it was not possible to reliably detect unacceptable seal counterfaces solely based on differences in friction behavior during clockwise and counterclockwise rotation. The newly developed test procedure revealed substantially different temporal friction profiles both between the various counterface systems and between the individual counterfaces of each system. The interpretation of these findings is further complicated by empirical knowledge that elastomeric rotary shaft seals can develop a preferred direction regarding their key functional parameters even on lead-free shafts due to run-in and wear processes, as well as further chemico-physical property changes of the seal lip during long-term operation. However, despite the uniqueness of the measured individual friction profiles, there are several relevant general findings. First, the observed friction differences clearly indicate that lead structures affect seal friction, with friction typically being higher during rotation in the reverse-pumping direction, where the lead structures partially drag lubricant out of the dynamic sealing gap, thereby reducing the lubricant film thickness. Furthermore, the friction torque difference (friction in the outward pumping (i. e., leakage) direction subtracted from that in the inward pumping direction) increases with decreasing sliding speed and lubricant viscosity, while the total friction torque decreases. Under such operating conditions with a reduced micro-elastohydrodynamic lubricant film thickness, which is governed by the product of speed and viscosity, the surface topography of the counterfaces obviously exhibits an increasing influence on the overall seal friction, possibly due to increased interaction between the surface structures/asperities and the elastomeric seal lip. This also explains the higher seal lip wear observed during rotation in the reverse-pumping direction. In systems that do not follow the aforementioned observations, increased friction instabilities and, in some cases, substantial leakage (e.g., system CF90) were observed.

While the particularly high shaft pump rates of the CF90 and CF100 systems may explain the leakage behavior of these systems, the leaking counterfaces of sizes CF50 exhibited pump rates that are below those of numerous leak-free systems. It is therefore not possible to reliably detect unacceptable seal counterfaces solely based on the results of shaft pump rate measurements.

Within the scope of this study, it was not possible to identify specific macro-lead parameters or thresholds that could be indicative of unacceptable counterfaces. This might be related to the fact that leakage in these systems was comparatively low, without exhibiting severe dripping leakage comparable to that of the CF90 micro-lead system. Micro-lead counterfaces exhibiting notable leakage had an average micro-lead angle Sd_{mean} of over 0.1 ° as well as shaft pump rates exceeding 0.02 mg/m. Moreover, micro-lead counterfaces with an average areal maximum height Sz_{mean} of approximately 2.5 µm or higher exhibited oil-wet sealing contacts or minor dripping leakage (system CF25), while the severely leaking CF90 systems exhibited markedly larger Sz_{mean} values between 2.8 and 3.5 µm. The suitability of these simple thresholds for predicting leakage in micro-lead shafts requires further study. Given that lead structures can exert a greater influence on the frictional behavior of sealing systems under unfavorable lubrication conditions (thin lubricant films due to low speed and/or lubricant viscosity), particular attention should be given to lead effects when using very low-viscosity lubricants in combination with reduced sliding speeds. Within the context of current development trends and research activities aimed at optimizing electrified powertrains, this particularly concerns elastomeric rotary shaft seals at the transmission output (see, for example, [29]).

5 Acknowledgements

The authors gratefully acknowledge the financial and technical support provided by the FVA – Research Association for Drive Technology within the framework of project FVA 805 II.

6 Nomenclature

Variable	***Description***	***Unit***
DP	Lead period length	m
Dt	Lead depth	m
Dy	Lead angle	°
PR_{CF}	Shaft (counterface) pump rate	mg/m
$PR_{Sys,cw}$	System pump rate in the clockwise direction	mg/m
$PR_{Sys,ccw}$	System pump rate in the counter-clockwise direction	mg/m
SDB_{mean}	Average structure width	m
SDT_{mean}	Average structure depth	m
SDy_{mean}	Average structure angle	°
Sd_{mean}	Average micro-lead angle	°
$Sz_{\ mean}$	Average areal maximum height	m
u	Sliding speed	m/s
η	Dynamic viscosity	Pa s

7 References

[1] Deutsches Institut für Normung e.V.: DIN 3761-1: Radial-Wellendichtringe für Kraftfahrzeuge - Begriffe; Maßbuchstaben; zulässige Abweichungen; Radialkraft, Berlin: Beuth. Januar 1984.

[2] Deutsches Institut für Normung e.V.: DIN 3760: Radial-Wellendichtringe, Berlin. September 1996.

[3] International Organization for Standardization: ISO 6194-1: Rotary shaft lip-type seals incorporating elastomeric sealing elements - Part 1: Nominal dimensions and tolerances. 15.09.2007.

[4] Rubber Manufacturers Association: Technical Bulletin RMA OS-1-1: Shaft Finish Requirements for Radial Lip Seals. 2004.

[5] Leis, A.; Hollen, J. von: Stochastische Strukturen - Auswirkungen stochastischer Strukturen von Gegenlaufflächen auf die Funktion von Radialwellendichtringen. Abschlussbericht FKM Forschungsvorhaben Nr. 281, Frankfurt/Main: FKM, 2010, Forschungskuratorium Maschinenbau e.V. (FKM).

[6] Matus, M.: Stochastische Strukturen. Auswirkung stochastischer Strukturen von Gegenlaufflächen auf die Funktion von Radialwellendichtringen. Abschlussbericht FVA Vorhaben Nr. 706 I, IGF-Nr. 17812 N, Frankfurt am Main: FVA, 2016, Forschungsvereinigung Antriebstechnik e.V. (FVA).

[7] Matus M.; Poll, G.: Stochastische Strukturen III: Auswirkung stochastischer Strukturen von Gegenlaufflächen auf die Funktion von Radialwellendichtringen; Forschungsvorhaben Nr. 706 II der FVA / Forschungsvereinigung Antriebstechnik e.V. Frankfurt a.M., Forschungsheft Nr. 1463, 2021.

[8] Matus, M. P.: Dichtheit von Radial-Wellendichtringen auf Gegenlaufflächen mit mesoskopischen Strukturen. Dissertation, Gottfried Wilhelm Leibniz Universität Hannover, 2023, doi:10.15488/14579.

[9] Lein, J.: Mechanische Untersuchungen an Dichtungsringen für rotierende Wellen, Berlin, Heidelberg: Springer Verlag, 1954, - ISBN 3662253356.

[10] Rau, N.; Seibold, M.: Verfahren zur Ermittlung einer Drallstruktur in der Oberflächenrauheit eines feinstbearbeiteten Wellenzapfens, 1997, Patentschrift, DE19740141C1.

[11] Seewig, J.; Hercke, T.: 2nd Generation Lead Measurement. XIX IMEKO World Congress, Lisbon, Portugal, September 6-11, 2009, 2009 - ISBN 9781615675937.

[12] Mercedes-Benz: Norm MBN 31007-7: Geometrische Produktspezifikationen (GPS) - Oberflächenbeschaffenheit Mess- und Auswerteverfahren zur Bewertung von drallreduzierten dynamischen Dichtflächen. September 2008.

[13] Raab, H.: Wellenlaufflächen. Einfluß der Wellenlauffläche auf das Dichtverhalten von Radial-Wellendichtringen. Abschlussbericht FKM Vorhaben Nr. 211, AiF-Nr. 10670, Frankfurt am Main: FKM, 1998, Forschungskuratorium Maschinenbau e.V. (FKM).

[14] Kunstfeld, T.: Einfluss der Wellenoberfläche auf das Dichtverhalten von Radial-Wellendichtungen. Dissertation, 2005, Universität Stuttgart, Institut für Maschinenelemente, - ISBN 3-936100-16-0.

[15] Buhl, S.: Wechselbeziehungen im Dichtsystem von Radial-Wellendichtring. Dissertation, 2006, Universität Stuttgart, Institut für Maschinenelemente, - ISBN 3-936100-18-7.

[16] Jung, S.: Beitrag zum Einfluss der Oberflächencharakteristik von Gegenlaufflächen auf das tribologische System Radial-Wellendichtung. Dissertation, 2013, Universität Stuttgart, Institut für Maschinenelemente, - ISBN 978-3-936100-42-6.

[17] Baitinger, G.; Haas, W.: Strukturanalyse. Drall- und Mikrostrukturanalyse zur funktionalen Bewertung von Dichtringgegenlaufflächen. Abschlussbericht FKM Vorhaben Nr. 285, AiF-Nr. 15628 N/1, Frankfurt am Main: FKM, 2011, Forschungskuratorium Maschinenbau e.V. (FKM).

[18] Baumann, M.; Bauer, F.; Haas, W.: Strukturanalyse II. Ganzheitliche, funktionale Bewertung von Dichtungsgegenlaufflächen mittels Strukturanalyse unter Einbeziehung der Wirkung von Strukturen auf die Förderwirkung der Welle. Abschlussbericht FKM Vorhaben Nr. 298, IGF-Nr. 17138 N/1, Frankfurt am Main: FKM, 2015, Forschungskuratorium Maschinenbau e.V. (FKM).

[19] Baumann, M.; Bauer, F.: Strukturanalyse III. Anwendung von Strukturanalyse und Festlegung von Qualitätskriterien für die gezielte Bewertung von Dichtungsgegenlaufflächen. Abschlussbericht FKM Vorhaben Nr. 308, IGF-Nr. 18186 N, Frankfurt am Main: FKM, 2017, Forschungskuratorium Maschinenbau e.V. (FKM).

[20] Engelfried, M.; Baumann, M.; Bauer, F.: 3D-Makrodrall - Strukturbasierte 3D-Analyse von Makrodrall. Forschungsheft 1471, Forschungsvereinigung Antriebstechnik e.V., Abschlussbericht FVA Vorhaben Nr. 876 I, Frankfurt am Main, 2022.

[21] Deutsches Institut für Normung e.V.: DIN 3761-1: Radial-Wellendichtringe für Kraftfahrzeuge - Begriffe; Maßbuchstaben; zulässige Abweichungen; Radialkraft, Berlin: Beuth. Januar 1984.

[22] Deutsches Institut für Normung e.V.: DIN 3760: Radial-Wellendichtringe, Berlin. September 1996.

[23] Poll, G.W.G.: A Contribution to the Discussion on Radial Lip Seal Working Principles. Radialwellendichtringe: III. Hamburger Dichtungstechnisches Kolloquium Dynamische Dichtungen, 2000.

[24] Wennehorst, B.: On Lubrication and Friction in Soft Rough Conformal Sliding Contacts. Experimental and theoretical contributions to the discussion on elastomer shaft seal tribology. Dissertation, 2016, Gottfried Wilhelm Leibniz Universität Hannover.

[25] Wennehorst, B.; Poll, G.: Soft micro-elastohydrodynamic lubrication and friction at rough conformal contacts. Proceedings of the Institution of Mechanical Engineers, Part J: Journal of Engineering Tribology 231, 3, pp. 302-315. DOI: https://doi.org/10.1177/1350650114558322, 2017.

[26] Kammüller, M.: Zum Abdichtverhalten von Radial-Wellendichtringen. Dissertation, 1986, Universität Stuttgart, Institut für Maschinenelemente, - ISBN 3-921920-19-1.

[27] Müller, H. K.: Concepts of Sealing Mechanism of Rubber Lip Type Rotary Shaft Seals. 11th International Conference on Fluid Sealing, Cannes, France; London, New York, USA: Elsevier, 1987, S. 698–709 - ISBN 9781851661008.

[28] Schiefer, F.; Matus, M.; Bauer, F.; Poll, G.: Schädliche Strukturen (Drall). Erkennen und Bewerten schädlicher Drallstrukturen auf RWDR-Gegenlaufflächen, Forschungsvereinigung Antriebstechnik e.V. (FVA), Forschungshefte // Forschungsvereinigung Antriebstechnik e.V. (FVA), Sachstandsbericht FVA Vorhaben Nr. 805 I, 2018.

[29] Lehnhardt, B.; Strobl, P.; Amro, M.; et al.: Tribologie elektrischer Hochdrehzahl-Antriebe. 65. GfT-Tribologie-Fachtagung „Reibung, Schmierung und Verschleiß“, Gesellschaft für Tribologie e.V. (GfT), 23.-25. September 2024, Göttingen.

8 Authors

Leibniz Universität Hannover, Institute of Machine Design and Tribology (IMKT)

An der Universität 1, 30823 Garbsen, Germany:

Mousa Amro, M. Sc.
amro@imkt.uni-hannover.de

Dr.-Ing. Bengt Wennehorst
wennehorst@imkt.uni-hannover.de

Prof. Dr.-Ing. Gerhard Poll, ORCID 0000-0002-3084-201X,
poll@imkt.uni-hannover.de

Prof. Dr.-Ing. Max Marian, ORCID 0000-0003-2045-6649,
marian@imkt.uni-hannover.de

https://doi.org/10.61319/WEABPFLT